

# Test-Time Adaptation via Cache Personalization for Facial Expression Recognition in Videos

Masoumeh Sharafi<sup>1</sup>, Muhammad Osama Zeeshan<sup>1</sup>, Soufiane Belharbi<sup>1</sup>,  
Alessandro Lameiras Koerich<sup>2</sup>, Marco Pedersoli<sup>1</sup>, and Eric Granger<sup>1</sup>

<sup>1</sup> LIVIA, Dept. of Systems Engineering, ETS Montreal, Canada

<sup>2</sup> LIVIA, Dept. of Software and IT Engineering, ETS Montreal, Canada  
{masoumeh.sharafi.1,muhammad-osama.zeeshan.1}@ens.etsmtl.ca  
{soufiane.belharbi, marco.pedersoli, alessandro.koerich,  
eric.granger}@etsmtl.ca

**Abstract.** Facial expression recognition (FER) in videos requires model personalization to capture the considerable variations across subjects. Vision-language models (VLMs) offer strong transfer to downstream tasks through image-text alignment, but their performance can still degrade under inter-subject distribution shifts. Personalizing models using test-time adaptation (TTA) methods can mitigate this challenge. However, most state-of-the-art TTA methods rely on unsupervised parameter optimization, introducing computational overhead that is impractical in many real-world applications. This paper introduces TTA through Cache Personalization (TTA-CaP), a cache-based TTA method that enables cost-effective (gradient-free) personalization of VLMs for video FER. Prior cache-based TTA methods rely solely on dynamic memories that store test samples, which can accumulate errors and drift due to noisy pseudo-labels. TTA-CaP leverages three coordinated caches – a personalized source cache that stores source-domain prototypes, a positive target cache that accumulates reliable subject-specific samples, and a negative target cache that stores low-confidence cases as negative samples to reduce the impact of noisy pseudo-labels. Cache updates and replacement are controlled by a tri-gate mechanism based on temporal stability, confidence, and consistency with the personalized cache. Finally, TTA-CaP refines predictions through fusion of embeddings, yielding refined representations that support temporally stable video-level predictions. Our experiments<sup>3</sup> on three challenging video FER datasets — BioVid, StressID, and BAH — indicate that TTA-CaP can outperform state-of-the-art TTA methods under subject-specific and environmental shifts, while maintaining low computational and memory overhead for real-world deployment.

**Keywords:** Emotion Recognition · Vision-Language Models · Gradient-Free Test-time Adaptation · Cache-Based Retrieval.

---

<sup>3</sup> Our code is publicly available at: [github.com/MasoumehSharafi/TTA-CaP](https://github.com/MasoumehSharafi/TTA-CaP).

## 1 Introduction

Video-based FER is a key component of various affective computing applications, such as human–computer interaction [27], health monitoring [11], and clinical assessment of pain, depression, and stress [3]. However, developing deep FER systems that perform well beyond controlled conditions remains challenging in video settings due to variability across capture conditions and expression dynamics. These challenges motivate the use of large-scale pre-trained models that remain effective for FER even with only a small amount of labeled data.

Large-scale VLMs such as contrastive language–image pre-training (CLIP) [28] have shown impressive transfer to downstream tasks by learning aligned image–text representations from web-scale data [18, 19, 42]. However, in video-based FER, their performance may still decline significantly at deployment (test time) under domain shift, particularly due to considerable variations in expressions across subjects and changes in acquisition conditions [33, 35]. This motivates the need for model *personalization*, i.e., adapting a FER model to the subtle expression patterns of a specific subject [30, 31, 44–46]. However, test-time personalization is typically performed on unlabeled video, where frame-level predictions can be noisy, especially during transitions and subtle low-intensity expressions. Although CLIP has recently been adapted for FER, most CLIP-based FER methods (e.g., EmoCLIP [9], DFER-CLIP [53], Exp-CLIP [52]) focus on subject-agnostic improvements to representations, prompting, or temporal modeling rather than online subject-level adaptation.

Personalization of VLMs through test-time adaptation (TTA) is largely underexplored for video FER. State-of-the-art TTA methods based on CLIP broadly fall into two groups. Prompt-tuning methods update prompts or lightweight modules at test time using unsupervised objectives such as entropy minimization and augmentation consistency [1, 8, 32, 41, 49]. However, these methods update model parameters through repeated backpropagation, leading to a notable increase in computational complexity. Cache-based TTA methods dynamically store target embeddings in a memory with their pseudo-labels to refine predictions through retrieval and fusion [5, 6, 13, 14, 16, 20, 23, 47, 48, 54]. Although cache-based methods have lower complexity (gradient-free), they rely solely on target-domain memories, which can accumulate errors and drift due to noisy pseudo-labels. We argue that accounting for subject-specific prototypes is an important source of information for accurate pseudo-labeling and personalization in video-based FER.

In this paper, we propose a cache-based gradient-free TTA method, called TTA via Cache Personalization (TTA-CaP), for cost-effective personalization of VLMs for video-based FER. As illustrated in Fig. 1(a), prior CLIP cache-based TTA methods are mainly image-based and typically rely on a dynamic target cache updated from pseudo-labels. They suffer from noisy pseudo-labels in videos, which lead to reduced performance. In contrast, TTA-CaP couples target caches with a personalized cache based on source subject prototypes (see Fig. 1(b)). Moreover, a tri-gate mechanism is introduced to update the two target caches during TTA. It filters updates based on (i) temporal stability across

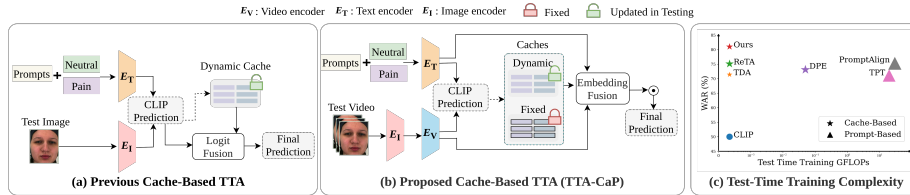


**Fig. 1: Left:** Comparison of SOTA cache-based TTA methods (a) against TTA-CaP (b). TTA-CaP adapts from a test video by combining a fixed personalized cache containing source domain prototypes with dynamic target-domain caches, and refines predictions via embedding-level fusion. (c) Average weighted average recall (WAR) versus test-time training GFLOPs on the BioVid dataset. Marker shape denotes cache- vs. prompt-based methods, and marker size indicates runtime (ms).

recent frames, (ii) prediction confidence via entropy, and (iii) consistency with the personalized cache. Feature-level fusion allows combining the CLIP visual embedding with cache-retrieved representations to obtain a refined embedding. Unlike logit-level fusion, which only adjusts class scores for the current sample, embedding-level fusion adapts the representation itself. This is more suitable for temporally aggregating embeddings into robust video-level decisions. Fig. 1 (c) shows the trade-off between accuracy and complexity for state-of-the-art TTA methods, highlighting that TTA-CaP improves performance while avoiding the computational overhead of prompt-tuning and cache-based methods.

Our contributions are summarized as follows. (1) We propose a cache-based, gradient-free TTA method, TTA-CaP, which couples target caches with a personalized source cache constructed from source subject prototypes to mitigate noisy pseudo-labels updates and refine predictions for personalized video FER. (2) We introduce a tri-gate mechanism to update the two target caches during TTA, along with an embedding-level fusion that combines CLIP visual representation with cache-retrieved representations to improve the reliability of predictions. (3) An extensive set of experiments on three challenging video FER benchmarks, BioVid [37] (pain estimation), StressID [4] (stress recognition), and BAH [12] (ambivalence-hesitancy recognition), showing that TTA-CaP can outperform state-of-the-art prompt-tuning and cache-based methods.

## 2 Related Work

**Vision-Language Models for FER.** VLMs trained with large-scale image-text contrastive learning (e.g., CLIP) enable prompt-based recognition by reframing classification as image-text matching [28] [28]. This is attractive for FER because expression classes are semantic, but FER is also fine-grained and entangled with identity and capture conditions, making performance sensitive to prompt design and inter-subject shift in realistic videos. Recent CLIP-based FER works improve the language interface and temporal modeling: CLIPER strengthens static and dynamic FER by leveraging multiple expression descrip-

tors to obtain more discriminative representations [17], while DFER-CLIP targets video FER by incorporating temporal modeling and enriched textual descriptions to better align subtle dynamics with language priors [53]. For zero-shot settings, EmoCLIP uses natural-language descriptions to improve generalization in video FER [9], and Exp-CLIP transfers task knowledge distilled from LLMs to enhance zero-shot recognition [52]. Beyond prompting, multimodal prompt alignment and parameter-efficient adaptation further refine CLIP-style models for dynamic FER [22]. Overall, these methods primarily advance prompting and training-time adaptation of VLMs, leaving open how to reliably adapt predictions at test time for videos.

**Test-Time Adaptation.** TTA mitigates distribution shift by updating a pre-trained model using only unlabeled test data at inference. Test-time training adapts via an auxiliary self-supervised objective but requires per-sample optimization [34]. Entropy-based methods such as Tent and MEMO improve robustness but still rely on iterative updates and can drift under noisy pseudo-labels or small batches [38, 50]. Subsequent approaches (EATA, SAR) aim to stabilize on-line adaptation, and continual variants (CoTTA, RoTTA) target non-stationary streams [25, 26, 39, 43]. Despite progress, prompt tuning TTA methods can remain sensitive to optimization choices and unreliable pseudo-labels, and its computational overhead can be restrictive for real-world deployment.

**Cache-Based TTA Methods.** Cache-based approaches augment a frozen backbone with an external memory and adapt predictions via feature retrieval in embedding space [16]. In the VLM setting, CLIP-Adapter and Tip-Adapter refine CLIP predictions using lightweight adapters or non-parametric key-value caches, with Tip-Adapter-F further improving performance through fine-tuning [10, 51]. Training-free neighbor-based variants such as CODER also leverage neighborhood structure to improve CLIP classification [40]. Recent test-time methods improve cache reliability via selective updates and calibration or prototype/statistics refinement [5, 6, 13, 20, 23, 47, 48, 54]. Despite these advances, existing cache-based TTA is not tailored to subject-based video FER: pseudo-label-driven target memories can degrade under frame-level noise, and most methods do not exploit subject-specific source priors to anchor class semantics, while long videos also raise memory and retrieval-cost concerns.

### 3 Proposed TTA-CaP Method

The proposed TTA-CaP method improves the model predictions by introducing a personalized source-domain cache as a fixed subject-specific reference, coupled with positive and negative target caches that store reliable and unreliable samples with their pseudo-labels, respectively. At test time, retrieved cache entries are combined with the current representation, and the same prompt-based head produces the final output prediction.

Fig. 2 summarizes the framework. Let  $\text{tgt}$  denote a target subject and  $\mathcal{X}^{\text{tgt}} = \{\mathbf{X}_t^{\text{tgt}}\}_{t=1}^T$  be an input video sequence of length  $T$ , where  $\mathbf{X}_t^{\text{tgt}} \in \mathbb{R}^{H \times W \times 3}$  denotes the RGB frame at time  $t$ . An image encoder  $E_1 : \mathbb{R}^{H \times W \times 3} \rightarrow \mathbb{R}^d$  maps

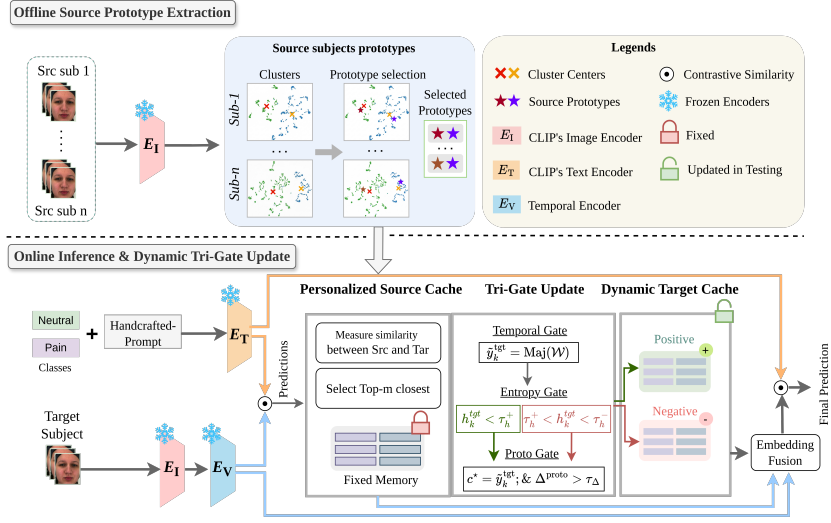


**Fig. 2:** Overview of our TTA-CaP. (top) **Offline source prototype extraction.** For each source-domain subject, CLIP image embeddings are clustered, and representative prototypes are selected to define a labeled set of source prototypes. (bottom) **Online TTA and tri-gate cache update.** At test time, frozen CLIP encoders produce text and visual embeddings and an initial prediction through contrastive similarity. A fixed personalized source cache retrieves the top- $m$  nearest source prototypes as a stable reference. A tri-gate controls updates to a dynamic target cache with positive and negative entries. Finally, predictions are obtained by embedding-level fusion of the CLIP visual embedding with retrieved cache items, enabling cost-effective personalization without training (backpropagation) at test-time.

each frame to a  $d$ -dimensional embedding:  $\mathbf{v}_t^{\text{tgt}} = E_I(\mathbf{X}_t^{\text{tgt}})$ . To model short-range temporal dynamics, we define a temporal encoder  $E_V : (\mathbb{R}^d)^L \rightarrow \mathbb{R}^d$ , which operates on a sliding window of length  $L$ . For  $t \geq L$ , the temporally aggregated representation is  $\mathbf{f}_t^{\text{tgt}} = E_V(\mathbf{v}_{t-L+1}^{\text{tgt}}, \dots, \mathbf{v}_t^{\text{tgt}})$ . Let  $\mathcal{C}$  denote the finite set of class labels. For each  $c \in \mathcal{C}$ , let  $p_c$  be a predefined textual prompt. A prompt-based CLIP text encoder  $E_T : \mathcal{P} \rightarrow \mathbb{R}^d$  produces normalized class embeddings  $\mathbf{e}_c$ . Given frozen CLIP encoders, classification logits at time  $t$  can be obtained via cosine similarity  $\ell_{t,c}^{\text{tgt}} = \mathbf{v}_t^{\text{tgt}\top} \mathbf{e}_c$ . The predicted label is  $\tilde{y}_t^{\text{tgt}} = \arg \max_{c \in \mathcal{C}} \ell_{t,c}^{\text{tgt}}(c)$ .

### 3.1 Personalized Source Cache

A fixed source cache is constructed *offline* and used at test time only for retrieval and reliability checks (no source-domain samples are accessed during adaptation). It stores a small set of source-derived prototypes (embeddings), selected to align the target subject in terms of feature statistics. For each class  $c \in \mathcal{C}$ , we maintain a fixed prototype  $\mathcal{P}_c^{\text{src,tgt}} \in \mathbb{R}^d$ .

**Offline source prototype extraction.** For each source subject and each class, embeddings are computed for all frames using the frozen image encoder  $E_I$ . These embeddings are then clustered with density-based spatial clustering of applications with noise (DBSCAN) to identify dense modes in feature space and to discard outliers as noise, following the original DBSCAN formulation [7]. DBSCAN depends on two parameters: a neighborhood radius and a minimum number of neighbors required to form a dense region. These parameters are selected separately for each subject–class subset to handle subject variability and class imbalance. Candidate settings are evaluated using two criteria: (i) basic clustering quality, favoring solutions with a low outlier rate and a non-degenerate cluster structure; and (ii) stability under bootstrap resampling, quantified by the mean adjusted rand index (ARI) across repeated runs, using standard ARI and clustering-stability references [2, 15, 29, 36]. After selecting the best-performing setting, each discovered cluster is summarized by a single prototype chosen as the sample closest to the cluster center. The set of these representatives constitutes the source prototypes.

**Personalized source cache construction.** A fixed source cache ( $\mathcal{P}_c^{\text{src,tgt}} \in \mathbb{R}^d$ ) is built for each target subject by selecting a subset of source subjects whose feature statistics are most similar to the target. Similarity is computed on an anchor subset of the target data (neutral) using a distributional (diagonal Fréchet) distance between anchor-feature distributions. After ranking source subjects by this criterion, prototypes from the top matched subjects (top- $m$ ) are pooled for each class to form the personalized source cache. This cache remains fixed during test time and serves as a stable reference for retrieval and reliability checks.

### 3.2 Online Dynamic Target Caches

During test time, two caches are created for the target subject to store information from the input samples: a positive cache for reliable samples and a negative cache for ambiguous cases.

**Positive cache.** For each target subject, a limited-capacity positive cache  $C^{\text{tgt}+}(t) = \{(\mathbf{z}_k^{\text{tgt}}, \tilde{y}_k^{\text{tgt}}, h_k^{\text{tgt}})\}_{k \in \mathcal{I}_t^+}$  stores reliable target samples at time  $t$ , where  $\mathbf{z}_k \in \mathbb{R}^d$  denotes a reliable pseudo-labeled embedding,  $\tilde{y}_k \in \mathcal{C}$  is its pseudo-label,  $h_k^{\text{tgt}}$  is the predictive uncertainty (entropy) measured at the time of insertion, and  $\mathcal{I}_t^+ \subseteq \{1, \dots, t\}$  indexes the insertion times. This cache is maintained per class with a fixed capacity to keep memory constant. When the capacity of a class-specific cache is exceeded, the least reliable entries (highest entropy) are removed, so the cache preserves high-confidence examples over time.

**Negative cache.** Similarly, for each target subject, we maintain a negative cache  $C^{\text{tgt}-}(t) = \{(\mathbf{z}_k^{\text{tgt}}, \tilde{y}_k^{\text{tgt}}, h_k^{\text{tgt}})\}_{k \in \mathcal{I}_t^-}$  stores information from uncertain samples. Each entry contains a frame embedding  $\mathbf{z}_k^{\text{tgt}}$  and a negative pseudo-label  $\tilde{y}_k$  indicating the least-likely class in that uncertain prediction. The cache is maintained per class with a fixed capacity. When a class-specific cache exceeds its capacity, higher-entropy entries are removed.

**Algorithm 1:** TTA-CaP (tri-gate cache update)

---

**Input** : frozen  $E_I, E_V, E_T$ ; prompts  $\{p_c\}$ ; fixed cache  $\mathcal{P}^{\mathcal{P}_c^{\text{src}, \text{tgt}}}$ ; target caches  $C^+, C^-$ ; window  $W$ ; thresholds  $(\tau_h^+, \tau_h^-, \tau_\Delta)$ .

**Output:** Updated target caches  $C^{\text{tgt}^+}(t)$  and  $C^{\text{tgt}^-}(t)$ .

$\{e_c\} \leftarrow E_T(\{p_c\})$ ;  
 Init  $C^{\text{tgt}^+}(t), C^{\text{tgt}^-}(t) \leftarrow \emptyset$ ;

**for**  $t = 1$  **to**  $T$  **do**

- $(\tilde{y}_k^{\text{tgt}}, h_t^{\text{tgt}}) \leftarrow \text{CLIPPREDICT}(\mathbf{v}_t^{\text{tgt}}, \{e_c\})$ ;
- if**  $\tilde{y}_t^{\text{tgt}} \neq \text{Maj}(\mathcal{W})$  **then**
- $\perp$  **continue**
- if**  $h_k^{\text{tgt}} < \tau_h^+$  **then**
- $\perp$   $\text{mode} \leftarrow +$
- else if**  $\tau_h^+ \leq h_k^{\text{tgt}} < \tau_h^-$  **then**
- $\perp$   $\text{mode} \leftarrow -$
- else**
- $\perp$  **continue**
- $(c^*, \Delta_{\text{proto}}) \leftarrow \text{PROTOMATCH}(\mathcal{P}^{\mathcal{P}_c^{\text{src}, \text{tgt}}}, \mathbf{v}_t^{\text{tgt}})$ ;
- if**  $(c^* = \tilde{y}_k^{\text{tgt}}) \ \& \ (\Delta_{\text{proto}} > \tau_\Delta)$  **then**
- if**  $\text{mode} = +$  **then**
- $\perp$   $\text{ADDPOS}(C^{\text{tgt}^+}(t), \mathbf{z}_k^{\text{tgt}}, \tilde{y}_k^{\text{tgt}}, h_k^{\text{tgt}})$
- else**
- $\perp$   $\text{ADDNEG}(C^{\text{tgt}^-}(t), \mathbf{z}_k^{\text{tgt}}, \tilde{y}_k^{\text{tgt}}, h_k^{\text{tgt}})$

---

### 3.3 Online TTA

Online adaptation is performed over the target video. At each time step  $t$ , an embedding  $\mathbf{v}_t^{\text{tgt}}$  is extracted, and CLIP prediction is obtained by comparing it to the class text embeddings  $\{\mathbf{e}_c\}_{c \in \mathcal{C}}$ . In parallel, the target caches are queried with the current frame embedding to retrieve relevant entries, which are fused with  $\mathbf{v}_t^{\text{tgt}}$  to refine the representation before producing the final prediction. Cache updates are then performed to store target samples with their pseudo-labels. Cache updates are controlled by a tri-gate mechanism, as shown in Algorithm 1: only reliable embeddings are stored in the positive or negative cache.

**Temporal gating.** Predictions in video FER can fluctuate due to motion, blur, or subtle expressions. To prevent cache updates from being triggered by such transient fluctuations, the temporal gate enforces short-term consistency: an update is accepted only if the current predicted label matches the majority label among the last  $W$  frames ( $\tilde{y}_k^{\text{tgt}} = \text{Maj}(\mathcal{W})$ ).

**Entropy gating.** Prediction confidence is measured using entropy of the predicted class distribution (lower entropy indicates higher confidence). Two entropy thresholds,  $\tau_h^+, \tau_h^-$ , are used to separate confident predictions from moderately uncertain ones. A prediction is treated as confident when  $h_k^{\text{tgt}} < \tau_h^+$ , and as uncertain when  $\tau_h^+ \leq h_k^{\text{tgt}} < \tau_h^-$ . Predictions with entropy above  $\tau_h^-$  are considered too uncertain and are not used for cache updates. This criterion is used because

cache updates should rely on reliable signals: high-entropy predictions are often noisy and can introduce incorrect entries. Using entropy thresholds limits updates to cases where the model is sufficiently confident, while still allowing moderately uncertain cases to be handled separately.

**Prototype gating.** A fixed personalized source cache provides class prototypes for the target subject. For the current embedding, similarity scores are computed to the prototypes of each class (using cosine similarity and averaging over the top- $k$  nearest prototypes). Let  $c^*$  be the prototype-based class suggestion (highest prototype similarity score) and let  $\Delta_{\text{proto}}$  be the margin between the best and second-best prototype similarity scores. The prototype consistency check passes only if  $c^* = \tilde{y}_k^{\text{tgt}}$  and  $\Delta_{\text{proto}} > \tau_{\Delta}$ , where  $\tilde{y}_k^{\text{tgt}}$  is the CLIP prediction.

**Cache update.** Since pseudo-labels can be noisy, cache updates are restricted to reliable cases: the temporal check avoids storing momentary prediction flips, and the prototype check avoids storing samples that disagree with the fixed source cache. When both checks pass, the entropy thresholds determine how the sample is stored. If the entropy is below  $\tau_h^+$ , the current embedding  $\mathbf{v}_t^{\text{tgt}}$  is added to the positive cache with its predicted label, treating it as reliable target information. If the entropy lies between  $\tau_h^+$  and  $\tau_h^-$ ,  $\mathbf{v}_t^{\text{tgt}}$  is added to the negative cache with a negative pseudo-label from that uncertain prediction, so ambiguous cases do not enter the positive cache. If the entropy is above  $\tau_h^-$ , no cache update is performed.

**Embedding-level fusion.** Fusion is performed in the CLIP embedding space rather than at the logit level. This preserves the cosine-similarity geometry used by CLIP and allows reuse of the same image-text similarity classifier. For each frame  $t$ , we form a refined target embedding by combining the current representation with retrieved source and target cache embeddings:

$$\mathbf{z}_t^{\text{tgt,fuse}} = \mathbf{z}_t^{\text{tgt}} + \mathbf{z}_t^{\text{src,tgt}} + \mathbf{z}_t^{\text{tgt+}} - \mathbf{z}_t^{\text{tgt-}}, \quad (1)$$

where  $\mathbf{z}_t^{\text{src,tgt}}$  is retrieved from the fixed personalized source cache,  $\mathbf{z}_t^{\text{tgt+}}$  from the positive target cache, and  $\mathbf{z}_t^{\text{tgt-}}$  from the negative target cache.

For each class  $c \in \mathcal{C}$ , we precompute a text embedding using the CLIP text encoder  $E_T$  and a class prompt  $\tau_c$ :

$$\mathbf{e}_c = \frac{E_T(\tau_c)}{\|E_T(\tau_c)\|_2}. \quad (2)$$

Given the fused frame embedding  $\mathbf{z}_t^{\text{tgt,fuse}}$ , frame-level logits are obtained by cosine similarity to the text embeddings:

$$\ell_t(c) = \eta \cos\left(\frac{\mathbf{z}_t^{\text{tgt,fuse}}}{\|\mathbf{z}_t^{\text{tgt,fuse}}\|_2}, \mathbf{e}_c\right), \quad \hat{y}_t = \arg \max_{c \in \mathcal{C}} \ell_t(c), \quad (3)$$

where  $\eta$  is the CLIP logit scale.

For a video of  $T$  frames, we aggregate frame-level logits by temporal averaging and predict the final label by argmax:

$$\bar{\ell}(c) = \frac{1}{T} \sum_{t=1}^T \ell_t(c), \quad \hat{y} = \arg \max_{c \in \mathcal{C}} \bar{\ell}(c). \quad (4)$$

**Table 1:** Comparison of the performance (F1 score and WAR) of zero-shot (ZS), fine-tuning (FT), and TTA on CLIP models for FER. Results are averaged over 10 target subjects for each dataset. CLIP-ViT-B/32<sup>†</sup> denotes full CLIP fine-tuning.

Protocol	Method	BioVid		StressID		BAH	
		WAR $\uparrow$	F1 $\uparrow$	WAR $\uparrow$	F1 $\uparrow$	WAR $\uparrow$	F1 $\uparrow$
ZS	CLIP-ViT-B/32 (ICML'21)	50.0	33.3	60.4	34.8	39.5	28.1
FT	CLIP-ViT-B/32 <sup>†</sup> (ICML'21)	69.7	66.6	67.0	44.5	60.4	39.8
	EmoCLIP [9] (FG'24)	67.7	63.4	63.5	35.9	56.2	36.5
	X-CLIP [24] (ECCV'22)	70.9	57.9	62.3	41.3	63.0	39.2
	Exp-CLIP [52] (WACV'25)	70.2	66.7	63.1	44.5	62.2	38.5
FT + TTA	TPT [32] (NeurIPS'22)	71.1	67.5	70.9	57.9	65.6	39.7
	TDA [16] (CVPR'24)	71.4	68.2	69.7	49.9	65.2	39.9
	DPE [48] (NeurIPS'24)	73.1	69.6	71.3	54.2	66.7	39.4
	PromptAlign [1] (NeurIPS'23)	75.3	71.6	74.6	53.2	67.1	39.7
	ReTA [20] (ACMMM'25)	75.1	71.3	71.8	52.8	67.6	39.8
	T3AL [21] (CVPR'24)	76.1	72.9	75.9	59.4	67.9	40.7
	TTA-CaP (ours)	<b>81.0</b>	<b>78.6</b>	<b>81.5</b>	<b>67.9</b>	<b>69.2</b>	<b>41.1</b>

## 4 Results and Discussion

### 4.1 Experimental Protocol

**Datasets.** Experiments are conducted on three challenging public video datasets: BioVid [37], StressID [4], and BAH [12]. Following prior work [31, 44–46], we use cross-subject splits between a source set (used to build fixed personalized prototypes) and a target set (used for TTA and inference). The BioVid heat pain database (Part A) contains controlled heat-pain recordings (multiple intensity levels and baseline) with synchronized facial video and physiological signals; we use 77 source subjects and 10 target subjects. StressID includes synchronized facial video, audio, and physiological measurements across stress-inducing tasks with self-reported affective ratings; we use 44 source subjects and 10 target subjects. BAH (behavioural ambivalence/hesitancy) is a large-scale multimodal dataset for ambivalence/hesitancy recognition collected via webcam/microphone with frame-level annotations; we use 143 source subjects and 10 target subjects.

**Implementation Details.** All experiments were conducted on a single NVIDIA A100 GPU (48 GB), using CLIP ViT-B/32 as the backbone. For constructing the personalized source cache, the top- $m=3$  closest source subjects are selected per target using a diagonal Fréchet distance on neutral-anchor embedding mean and diagonal variance. Online TTA uses a temporal window length  $\mathcal{W}=3$ , and prototype margin threshold  $\tau_{\Delta}=0.05$ . The positive cache capacity is set to 5 with  $\tau_h^+=0.5$ , and the negative cache capacity is set to 4 with  $\tau_h^-=0.8$ .

**Baseline Methods.** Following the baseline CLIP-based FER and TTA methods [1, 9, 16], all results are reported using two standard metrics: weighted average recall (WAR), which corresponds to overall classification accuracy, and F1 score, which balances precision and recall under class imbalance. Baseline comparisons cover both CLIP-based FER approaches and different TTA methods. For CLIP-based FER, TTA-CaP is evaluated against the frozen CLIP-ViT-B/32

**Table 2:** Subject-wise performance (F1 score) on the BioVid dataset for TTA-CaP and other TTA methods. Best F1 scores are highlighted in bold.

Method	Sub-1	Sub-2	Sub-3	Sub-4	Sub-5	Sub-6	Sub-7	Sub-8	Sub-9	Sub-10	Avg.
TPT [32]	92.0	51.5	40.0	49.6	79.0	87.0	79.5	43.4	99.0	54.0	67.5
TDA [16]	94.9	50.3	43.5	48.0	80.8	86.2	80.2	43.5	<b>100.0</b>	55.0	68.2
DPE [48]	90.4	51.5	43.5	73.1	72.0	83.6	79.8	48.5	<b>100.0</b>	54.4	69.6
PromptAlign [1]	94.2	60.1	42.5	61.5	83.5	90.5	80.2	43.5	<b>100.0</b>	60.0	71.6
ReTA [20]	94.2	60.1	43.5	60.8	83.5	88.0	80.2	43.5	<b>100.0</b>	60.0	71.3
T3AL [21]	<b>95.8</b>	62.0	<b>43.9</b>	61.5	83.9	93.9	83.0	43.5	<b>100.0</b>	62.0	72.9
TTA-CaP (ours)	94.3	<b>66.3</b>	33.3	<b>73.2</b>	<b>100.0</b>	<b>97.4</b>	<b>89.8</b>	<b>47.8</b>	<b>100.0</b>	<b>84.0</b>	<b>78.6</b>

**Table 3:** Subject-wise performance (F1 score) on the StressID dataset for TTA-CaP and other TTA methods. Best F1 scores are highlighted in bold.

Method	Sub-1	Sub-2	Sub-3	Sub-4	Sub-5	Sub-6	Sub-7	Sub-8	Sub-9	Sub-10	Avg.
TPT [32]	70.7	43.6	86.0	<b>83.1</b>	36.4	78.7	41.1	50.0	40.0	50.0	57.9
TDA [16]	45.5	40.0	50.1	81.0	35.0	80.0	29.6	45.6	42.9	50.0	49.9
DPE [48]	41.0	40.6	49.0	81.0	49.8	80.0	56.0	46.0	42.9	56.6	54.2
PromptAlign [1]	41.3	45.0	45.6	82.3	48.1	80.0	44.0	58.0	42.9	45.5	53.2
ReTA [20]	43.2	41.0	53.0	80.9	36.1	80.0	39.1	53.3	42.9	59.3	52.8
T3AL [21]	46.3	48.6	48.6	80.1	<b>51.0</b>	80.0	61.8	68.0	44.0	66.0	59.4
TTA-CaP (ours)	<b>77.4</b>	<b>50.0</b>	<b>89.1</b>	82.0	44.4	<b>87.8</b>	<b>62.0</b>	<b>68.8</b>	<b>47.0</b>	<b>70.8</b>	<b>67.9</b>

**Table 4:** Subject-wise performance (F1 score) on the BAH dataset for TTA-CaP and other TTA methods. Best F1 scores are highlighted in bold.

Method	Sub-1	Sub-2	Sub-3	Sub-4	Sub-5	Sub-6	Sub-7	Sub-8	Sub-9	Sub-10	Avg.
TPT [32]	40.6	35.7	43.7	45.9	45.6	43.1	35.0	34.7	40.7	32.9	39.7
TDA [16]	40.0	39.7	44.4	46.0	42.0	42.6	35.0	35.5	40.7	33.2	39.9
DPE [48]	34.8	37.1	44.2	46.0	45.3	43.0	37.2	32.5	<b>41.0</b>	33.2	39.4
PromptAlign [1]	25.0	37.0	46.9	51.0	46.1	43.5	41.0	32.5	<b>41.0</b>	33.2	39.7
ReTA [20]	25.0	36.9	41.9	51.0	46.1	51.2	40.0	32.5	<b>41.0</b>	33.2	39.8
T3AL [21]	41.6	37.0	44.7	46.0	45.2	43.0	38.0	<b>36.2</b>	<b>41.0</b>	35.0	40.7
TTA-CaP (ours)	<b>41.9</b>	<b>39.9</b>	<b>44.7</b>	<b>46.2</b>	<b>46.1</b>	<b>43.6</b>	<b>41.0</b>	32.2	40.4	<b>35.2</b>	<b>41.1</b>

backbone (zero-shot), CLIP-ViT-B/32<sup>†</sup> [9] (CLIP fine-tuned on source), and EmoCLIP [9] (adapter-only training). Additional baselines include X-CLIP [24] and Exp-CLIP [52], which incorporate trainable projection modules and for Exp-CLIP, LLM-derived facial-expression descriptions as supervision. For TTA, TTA-CaP is compared against representative methods originally proposed for image recognition, including TPT [32], TDA [16], DPE [48], PromptAlign [1], and ReTA [20], together with an adaptation of the video-based action recognition method T3AL [21]. All methods share the same CLIP backbone and prompting scheme, and are evaluated under identical preprocessing and protocols. For all TTA baselines and TTA-CaP, the prompt template “*a person with an expression of /CLS/*” is used, following prior CLIP-based FER work [52]. Additional details on baseline methods and prompt selection are provided in the supplementary materials.

## 4.2 Comparison with State-of-the-Art Methods

Table 1 compares CLIP-based FER baselines, fine-tuning variants, and state-of-the-art TTA methods on BioVid, StressID, and BAH datasets. Across all datasets, moving from CLIP inference to adaptation (either via fine-tuning or test-time updates) generally improves recognition under personalized expression styles and domain shift. In particular, TTA methods tend to yield larger gains when target subjects deviate from source distributions, highlighting the importance of online personalization beyond a fixed encoder.

Within TTA approaches, methods differ in how they trade accuracy for test-time cost. Prompt-based optimization can be effective but typically incurs higher runtime and memory overhead, whereas cache-based adaptation improves efficiency by reusing confident target evidence. In this context, TTA-CaP achieves strong performance while remaining lightweight: it attains 81.0/78.6 (WAR/F1 score) on BioVid, 81.5/67.9 on StressID, and 69.2/41.1 on BAH, while preserving a favorable runtime–memory profile (Table 5). This suggests that the gains are not solely driven by frequent classes (WAR), but also translate to improved class-balanced performance (F1 score), which is critical under imbalanced labels and heterogeneous subject expression styles.

The subject-wise results (Tables 2–4) further clarify these trends. On BioVid and StressID, adaptation consistently reduces subject-to-subject variability: while prior methods can fluctuate on challenging target subjects, the overall behavior becomes more stable with personalized test-time evidence. On BAH, performance is generally lower and margins between methods are smaller, which is likely due to less controlled face capture conditions that amplify appearance and motion variability. Overall, these results suggest that personalization should be assessed not only by aggregate metrics but also by subject-level consistency, and that TTA-CaP provides a strong accuracy–efficiency trade-off among CLIP-based TTA approaches. Due to space constraints, subject-wise F1 score for all 10 target subjects on each dataset is reported in the main paper; complete subject-wise results including WAR and UAR for all datasets, as well as subject-wise results for CLIP-based FER baselines, are provided in the supplementary materials.

## 4.3 Qualitative Visualization

Quantitative results are complemented with qualitative visualizations that illustrate how TTA-CaP behaves during online TTA, with a focus on representation structure and the dynamics of the tri-gate reliability rule. The t-SNE embedding projection in Fig. 3 (left) provides a qualitative view of class structure in the learned representation. The plot shows embeddings before and after cache fusion for two subjects from StressID dataset, with points colored by class (Neutral vs. Stress). After cache fusion, the two classes occupy more distinct regions with reduced overlap, indicating improved separability in the feature space and fewer boundary ambiguities.

Fig. 3 (right) reports the gate cascade pass rates, summarizing how often each reliability criterion is satisfied over time, *i.e.* the fraction of frames that pass a

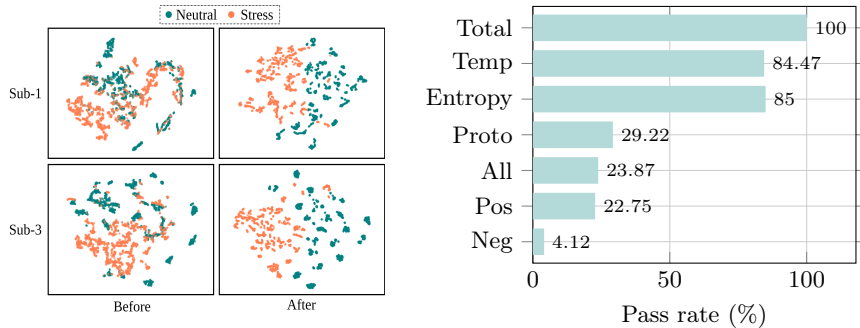


**Fig. 3: Qualitative visualization.** Left: t-SNE visualization of the embedding space *before/after* cache fusion for two subjects from **StressID**. Right: gate pass rates (fraction of frames passing each criterion and updating the caches).

given gate and therefore remain eligible to update the caches. The temporal and entropy gates exhibit high pass rates (84.47% and 85.0%), indicating stable and confident predictions, whereas the prototype gate is more selective (29.22%), reflecting the role of the source-anchored reference in enforcing semantic agreement and decisiveness. When all criteria are enforced jointly, only 23.87% of frames trigger an update *All*, yielding conservative long-horizon adaptation. This selectivity propagates to the cache-specific updates: 22.75% of frames are admitted into the positive cache, while the negative cache is updated rarely (4.12%), consistent with its intended use as sparse counter-evidence rather than a frequently refreshed memory.

#### 4.4 Computation Complexity

Table 5 reports the per-batch runtime (ms), memory (MB), and average WAR (%) on the BioVid dataset. Overall, TTA-CaP achieves the best accuracy while keeping the test-time cost low. In particular, TTA-CaP is faster than prompt-tuning TTA methods (e.g., TPT and PromptAlign), since it avoids backpropagation and instead performs a small number of encoder forward passes, cache retrievals, and a lightweight fusion step. As a result, TTA-CaP offers a markedly improved accuracy–efficiency trade-off over existing TTA baselines, improving WAR while maintaining low runtime and memory.

#### 4.5 Ablation Studies

**Ablation on Cache-Update Gating.** We analyze the effect of cache-update gating by enabling different subsets of the three reliability criteria. Using entropy-only gating yields 75.2 WAR. Adding temporal stability (Temp+Entropy) improves robustness and increases performance to 78.3 WAR. When entropy is disabled, the two-gate variants perform worse: Temp+Proto reaches 76.0 WAR, while Entropy+Proto achieves 77.8 WAR. Enabling the full tri-gate achieves the best

**Table 5:** Complexity of TTA methods. Run time per batch (B=16), memory, and average WAR for BioVid target subjects.

Method	Time (ms)	Mem. (MB)	WAR (%)
TPT	771.2	2800	71.1
PromptAlign	900.0	3100	75.3
TDA	<b>97.8</b>	2124	71.4
DPE	263.9	1700	73.1
ReTA	174.0	2390	75.1
T3AL	520.0	2200	76.1
TTA-CaP	110.0	<b>904.0</b>	<b>81.0</b>

**Table 6:** Ablation of cache-update gating in TTA-CaP. Average WAR over BioVid target subjects for different gate settings.

Temp.	Entropy	Proto.	WAR (%) $\uparrow$
$\times$	$\checkmark$	$\times$	75.2
$\checkmark$	$\checkmark$	$\times$	78.3
$\checkmark$	$\times$	$\checkmark$	76.0
$\times$	$\checkmark$	$\checkmark$	77.8
$\checkmark$	$\checkmark$	$\checkmark$	<b>81.0</b>

result of 81.0 WAR. Overall, Table 6 shows that entropy-based filtering is essential, temporal consistency complements confidence-based updates, and prototype-consistency provides additional gains when combined with both.

**Impact of Subject Selection for Personalized Source Cache.** Fig. 4 shows the effect of selecting the top- $m$  most similar source subjects to build the personalized source cache for TTA-CaP. On BioVid, performance increases steadily from  $m=0$  to  $m=3$  and then saturates, indicating that a small number of well-matched source subjects provides strong prototype anchors while additional subjects yield diminishing returns. A similar trend is observed on StressID and BAH: WAR improves markedly when moving from  $m=0$  to  $m \leq 2-3$ , followed by a plateau, suggesting that the benefit comes primarily from incorporating a few closely aligned source subjects rather than expanding the cache with less relevant variability.

**Ablation on Cache Design.** We analyze the contribution of the proposed static personalized source cache (prototype-based anchor) relative to the dynamic target cache (positive/negative memory). As shown in Fig. 5a, starting from a low CLIP baseline of 50.0 WAR, using the static cache alone increases performance to 75.5 WAR, indicating that source prototypes provide a strong target data-free prior even without online updates. The dynamic cache alone achieves 78.0 WAR, reflecting the benefit of accumulating target-specific evidence over the stream.

Combining static and dynamic caches yields the best result of 81.0 WAR, improving over dynamic-only by +3 WAR. This suggests that the static cache is not redundant; rather, it complements target memory by anchoring class semantics and stabilizing online adaptation under severe domain/personalization shift.

**Source-Cache Generation Strategy.** The effect of source cache without using source data construction is analyzed under the same online TTA pipeline and cache budget. We studied four different methods to build the static cache prototypes: (i) GMM virtual prototypes sampled around class centers (classifier-

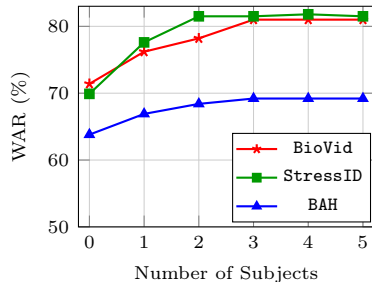


**Fig. 4:** Impact of selecting the top- $m$  most similar source subjects for the personalized source cache (WAR on target subjects).

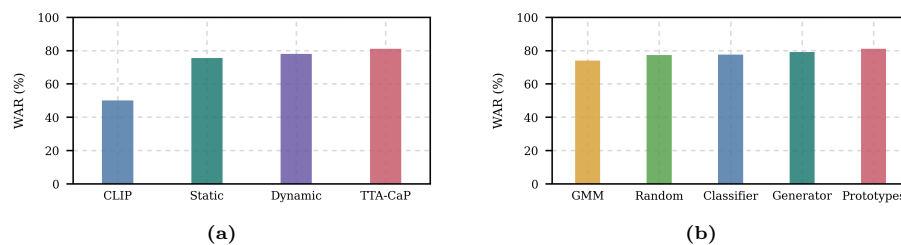


**Fig. 5:** (a) Average WAR for target subjects in BioVid for zero-shot CLIP, static personalized source cache only, dynamic target cache only, and TTA-CaP (static + dynamic). (b) Ablation of source-cache construction in BioVid. Average WAR across target subjects. Prototypes: the personalized source cache built from source-subject prototypes.

weight anchors), (ii) random sampling in the embedding space with pseudo-labeling by the frozen classifier, (iii) classifier prototypes using the classifier weights directly as class anchors, and (iv) a generator-based feature-space model that produces class-conditional avatar prototypes. Fig. 5b shows that more class-consistent source prototypes yield stronger downstream adaptation: the generator-based source cache performs best among data-free strategies (WAR = 79.1), while GMM perturbations around class centers are less effective (WAR = 74.0). For comparison, the full TTA-CaP configuration with personalized source-subject prototypes (“Prototypes” in the figure) achieves WAR = 81.0, indicating that higher-quality source prototypes provide a strong foundation and are further strengthened when combined with the complete cache design.

## 5 Conclusion

This paper proposed TTA-CaP, a gradient-free cache-based TTA method for cost-effective personalization of CLIP-based video FER. TTA-CaP combines two target dynamic caches with a fixed personalized source cache built from source-subject prototypes to improve subject-specific adaptation at test time. Moreover, a tri-gate reliability mechanism is introduced to update the target caches and refine predictions via feature-level fusion with retrieved cache entries. Experiments on BioVid, StressID, and BAH datasets show consistent gains in both WAR and F1 over prompt-tuning and cache-based baselines, while preserving low test-time computation and bounded memory. As future work, we will investigate fully online personalized cache construction and extend TTA-CaP to other video behavior recognition tasks (e.g., actions, gestures, events, and affect recognition).

**Supplementary materials.** Includes additional personalization results for CLIP-based FER and TTA methods with WAR, UAR, and F1 score, detailed baselines, implementation settings, prompt selection, algorithms for personalized source-cache construction and online TTA, and extended ablation studies.

## References

1. Abdul Samadh, J., Gani, M.H., Hussein, N., Khattak, M.U., Naseer, M.M., Shahbaz Khan, F., Khan, S.H.: Align your prompts: Test-time prompting with distribution alignment for zero-shot generalization. *Advances in Neural Information Processing Systems* **36**, 80396–80413 (2023) [2](#), [9](#), [10](#)
2. Ben-Hur, A., Elisseeff, A., Guyon, I.: A stability based method for discovering structure in clustered data. In: *Biocomputing 2002*, pp. 6–17. World Scientific (2001) [6](#)
3. Calvo, R.A., D’Mello, S.: Affect detection: An interdisciplinary review of models, methods, and their applications. *IEEE Transactions on Affective Computing* **1**(1), 18–37 (2010) [2](#)
4. Chaptoukaev, H., Strizhkova, V., Panariello, M., Dalpaos, B., Reka, A., Manera, V., Thümmler, S., Ismailova, E., Todisco, M., Zuluaga, M.A., et al.: Stressid: a multimodal dataset for stress identification. *Advances in Neural Information Processing Systems* **36**, 29798–29811 (2023) [3](#), [9](#)
5. Chen, S., Chen, Y., Yin, X., Liu, X., Lai, H., Zhang, T.: Paf: Prototype adaptive fusion for test-time adaptation of vision-language models. In: *Proceedings of the 33rd ACM International Conference on Multimedia*. pp. 3007–3016 (2025) [2](#), [4](#)
6. Chen, X., Zhai, H., Zhang, C., Shi, X., Li, R.: Multi-cache enhanced prototype learning for test-time generalization of vision-language models. In: *Proceedings of the IEEE/CVF International Conference on Computer Vision*. pp. 2281–2291 (2025) [2](#), [4](#)
7. Ester, M., Kriegel, H.P., Sander, J., Xu, X., et al.: A density-based algorithm for discovering clusters in large spatial databases with noise. In: *kdd*. vol. 96, pp. 226–231 (1996) [6](#)
8. Feng, C.M., Yu, K., Liu, Y., Khan, S., Zuo, W.: Diverse data augmentation with diffusions for effective test-time prompt tuning. In: *Proceedings of the IEEE/CVF International Conference on Computer Vision*. pp. 2704–2714 (2023) [2](#)
9. Foteinopoulou, N.M., Patras, I.: Emoclip: A vision-language method for zero-shot video facial expression recognition. In: *2024 IEEE 18th International Conference on Automatic Face and Gesture Recognition (FG)*. pp. 1–10. IEEE (2024) [2](#), [4](#), [9](#), [10](#)
10. Gao, P., Geng, S., Zhang, R., Ma, T., Fang, R., Zhang, Y., Li, H., Qiao, Y.: Clip-adapter: Better vision-language models with feature adapters. *International Journal of Computer Vision* **132**(2), 581–595 (2024) [4](#)
11. Gaya-Morey, F.X., Buades-Rubio, J.M., Palanque, P., Lacuesta, R., Manresa-Yee, C.: Deep learning-based facial expression recognition for the elderly: A systematic review. *arXiv preprint arXiv:2502.02618* (2025) [2](#)
12. González-González, M., Belharbi, S., Zeeshan, M.O., Sharafi, M., Aslam, M.H., Pedersoli, M., Koerich, A.L., Bacon, S.L., Granger, E.: Bah dataset for ambivalence/hesitancy recognition in videos for behavioural change. *arXiv preprint arXiv:2505.19328* (2025) [3](#), [9](#)
13. Guan, Z., Yucan, Z., Liu, W., Gu, X.: Statistics caching test-time adaptation for vision-language models. In: *The Thirty-ninth Annual Conference on Neural Information Processing Systems* (2025) [2](#), [4](#)
14. Huang, F., Jiang, J., Jiang, Q., Li, H., Khan, F.N., Wang, Z.: Cosmic: Clique-oriented semantic multi-space integration for robust clip test-time adaptation. In: *Proceedings of the Computer Vision and Pattern Recognition Conference*. pp. 9772–9781 (2025) [2](#)

15. Hubert, L., Arabie, P.: Comparing partitions. *Journal of classification* **2**(1), 193–218 (1985) [6](#)
16. Karmanov, A., Guan, D., Lu, S., El Saddik, A., Xing, E.: Efficient test-time adaptation of vision-language models. In: *Proceedings of the IEEE/CVF Conference on Computer Vision and Pattern Recognition*. pp. 14162–14171 (2024) [2](#), [4](#), [9](#), [10](#)
17. Li, H., Niu, H., Zhu, Z., Zhao, F.: Cliper: A unified vision-language framework for in-the-wild facial expression recognition. In: *2024 IEEE International Conference on Multimedia and Expo (ICME)*. pp. 1–6. IEEE (2024) [4](#)
18. Li, J., Li, D., Savarese, S., Hoi, S.: Blip-2: Bootstrapping language-image pre-training with frozen image encoders and large language models. In: *International conference on machine learning*. pp. 19730–19742. PMLR (2023) [2](#)
19. Li, Y., Liang, F., Zhao, L., Cui, Y., Ouyang, W., Shao, J., Yu, F., Yan, J.: Supervision exists everywhere: A data efficient contrastive language-image pre-training paradigm. *arXiv preprint arXiv:2110.05208* (2021) [2](#)
20. Liang, Y., Chen, H., Xiong, Y., Zhou, Z., Lyu, M., Lin, Z., Niu, S., Zhao, S., Han, J., Ding, G.: Advancing reliable test-time adaptation of vision-language models under visual variations. In: *Proceedings of the 33rd ACM International Conference on Multimedia*. pp. 4788–4797 (2025) [2](#), [4](#), [9](#), [10](#)
21. Liberatori, B., Conti, A., Rota, P., Wang, Y., Ricci, E.: Test-time zero-shot temporal action localization. In: *Proceedings of the IEEE/CVF conference on computer vision and pattern recognition*. pp. 18720–18729 (2024) [9](#), [10](#)
22. Ma, F., He, Y., Sun, B., Li, S.: Multimodal prompt alignment for facial expression recognition. In: *IEEE/CVF International Conference on Computer Vision (ICCV)* (2025) [4](#)
23. Nguyen, K.B., Bui, P.N., Choo, H., Nguyen, D.T.: Adaptive cache enhancement for test-time adaptation of vision-language models. *arXiv preprint arXiv:2508.07570* (2025) [2](#), [4](#)
24. Ni, B., Peng, H., Chen, M., Zhang, S., Meng, G., Fu, J., Xiang, S., Ling, H.: Expanding language-image pretrained models for general video recognition. In: *European Conference on Computer Vision*. pp. 1–18 (2022) [9](#), [10](#)
25. Niu, S., Wu, J., Zhang, Y., Chen, Y., Zheng, S., Zhao, P., Tan, M.: Efficient test-time model adaptation without forgetting. In: *International conference on machine learning*. pp. 16888–16905. PMLR (2022) [4](#)
26. Niu, S., Wu, J., Zhang, Y., Wen, Z., Chen, Y., Zhao, P., Tan, M.: Towards stable test-time adaptation in dynamic wild world. In: *International Conference on Learning Representations (ICLR)* (2023) [4](#)
27. Pu, J., Nie, X.: Convolutional channel attentional facial expression recognition network and its application in human-computer interaction. *IEEE Access* **11**, 129412–129424 (2023) [2](#)
28. Radford, A., Kim, J.W., Hallacy, C., Ramesh, A., Goh, G., Agarwal, S., Sastry, G., Askell, A., Mishkin, P., Clark, J., et al.: Learning transferable visual models from natural language supervision. In: *International conference on machine learning*. pp. 8748–8763. PmLR (2021) [2](#), [3](#)
29. Rand, W.M.: Objective criteria for the evaluation of clustering methods. *Journal of the American Statistical association* **66**(336), 846–850 (1971) [6](#)
30. Sharafi, M., Belharbi, S., Salem, H.B., Etemad, A., Koerich, A.L., Pedersoli, M., Bacon, S., Granger, E.: Personalized feature translation for expression recognition: An efficient source-free domain adaptation method. *arXiv preprint arXiv:2508.09202* (2025) [2](#)

31. Sharafi, M., Ollivier, E., Zeeshan, M.O., Belharbi, S., Koerich, A.L., Pedersoli, M., Bacon, S., Granger, E.: Disentangled source-free personalization for facial expression recognition with neutral target data. In: 2025 IEEE 19th International Conference on Automatic Face and Gesture Recognition (FG). pp. 1–10. IEEE (2025) [2](#), [9](#)
32. Shu, M., Nie, W., Huang, D.A., Yu, Z.: Test-time prompt tuning for zero-shot generalization in vision-language models. *Advances in Neural Information Processing Systems* **35**, 14274–14289 (2022) [2](#), [9](#), [10](#)
33. Shu, Y., Guo, X., Wu, J., Wang, X., Wang, J., Long, M.: Clipood: Generalizing clip to out-of-distributions. In: International conference on machine learning. pp. 31716–31731. PMLR (2023) [2](#)
34. Sun, Y., Wang, X., Liu, Z., Miller, J., Efros, A., Hardt, M.: Test-time training with self-supervision for generalization under distribution shifts. In: International conference on machine learning. pp. 9229–9248. PMLR (2020) [4](#)
35. Tu, W., Deng, W., Gedeon, T.: A closer look at the robustness of contrastive language-image pre-training (clip). *Advances in Neural Information Processing Systems* **36**, 13678–13691 (2023) [2](#)
36. Vinh, N.X., Epps, J., Bailey, J.: Information theoretic measures for clusterings comparison: Variants, properties, normalization and correction for chance. *Journal of Machine Learning Research* **11**, 2837–2854 (2010) [6](#)
37. Walter, S., Gruss, S., Ehleiter, H., Tan, J., Traue, H.C., Werner, P., Al-Hamadi, A., Crawcour, S., Andrade, A.O., da Silva, G.M.: The biovid heat pain database data for the advancement and systematic validation of an automated pain recognition system. In: 2013 IEEE international conference on cybernetics (CYBCO). pp. 128–131. IEEE (2013) [3](#), [9](#)
38. Wang, D., Shelhamer, E., Liu, S., Olshausen, B., Darrell, T.: Tent: Fully test-time adaptation by entropy minimization. *arXiv preprint arXiv:2006.10726* (2020) [4](#)
39. Wang, Q., Fink, O., Van Gool, L., Dai, D.: Continual test-time domain adaptation. In: Proceedings of the IEEE/CVF Conference on Computer Vision and Pattern Recognition. pp. 7201–7211 (2022) [4](#)
40. Yi, C., Ren, L., Zhan, D.C., Ye, H.J.: Leveraging cross-modal neighbor representation for improved clip classification. In: Proceedings of the IEEE/CVF Conference on Computer Vision and Pattern Recognition. pp. 27402–27411 (2024) [4](#)
41. Yoon, H.S., Yoon, E., Tee, J.T.J., Hasegawa-Johnson, M., Li, Y., Yoo, C.D.: C-tp: Calibrated test-time prompt tuning for vision-language models via text feature dispersion. *arXiv preprint arXiv:2403.14119* (2024) [2](#)
42. Yu, J., Wang, Z., Vasudevan, V., Yeung, L., Seyedhosseini, M., Wu, Y.: Coca: Contrastive captioners are image-text foundation models. *arXiv preprint arXiv:2205.01917* (2022) [2](#)
43. Yuan, L., Xie, B., Li, S.: Robust test-time adaptation in dynamic scenarios. In: Proceedings of the IEEE/CVF Conference on Computer Vision and Pattern Recognition. pp. 15922–15932 (2023) [4](#)
44. Zeeshan, M.O., Aslam, M.H., Belharbi, S., Koerich, A.L., Pedersoli, M., Bacon, S., Granger, E.: Subject-based domain adaptation for facial expression recognition. In: 2024 IEEE 18th International Conference on Automatic Face and Gesture Recognition (FG). pp. 1–10. IEEE (2024) [2](#), [9](#)
45. Zeeshan, M.O., Gillet, N., Koerich, A.L., Pedersoli, M., Bremond, F., Granger, E.: Musaco: Multimodal subject-specific selection and adaptation for expression recognition with co-training. *arXiv preprint arXiv:2508.12522* (2025) [2](#), [9](#)

46. Zeeshan, M.O., Pedersoli, M., Koerich, A.L., Granger, E.: Progressive multi-source domain adaptation for personalized facial expression recognition. *IEEE Transactions on Affective Computing* (2025) [2](#), [9](#)
47. Zhai, H., Chen, X., Zhang, C., Sha, T., Li, R.: Mitigating cache noise in test-time adaptation for large vision-language models. In: 2025 IEEE International Conference on Multimedia and Expo (ICME). pp. 1–6. IEEE (2025) [2](#), [4](#)
48. Zhang, C., Stepputtis, S., Sycara, K., Xie, Y.: Dual prototype evolving for test-time generalization of vision-language models. *Advances in Neural Information Processing Systems* **37**, 32111–32136 (2024) [2](#), [4](#), [9](#), [10](#)
49. Zhang, D.C., Zhou, Z., Li, Y.F.: Robust test-time adaptation for zero-shot prompt tuning. In: *Proceedings of the AAAI Conference on Artificial Intelligence*. vol. 38, pp. 16714–16722 (2024) [2](#)
50. Zhang, M., Levine, S., Finn, C.: Memo: Test time robustness via adaptation and augmentation. *Advances in neural information processing systems* **35**, 38629–38642 (2022) [4](#)
51. Zhang, R., Zhang, W., Fang, R., Gao, P., Li, K., Dai, J., Qiao, Y., Li, H.: Tip-adapter: Training-free adaption of clip for few-shot classification. In: *European conference on computer vision*. pp. 493–510. Springer (2022) [4](#)
52. Zhao, Z., Cao, Y., Gong, S., Patras, I.: Enhancing zero-shot facial expression recognition by llm knowledge transfer. in 2025 *iee/cvf winter conference on applications of computer vision (wacv)* (2025) [2](#), [4](#), [9](#), [10](#)
53. Zhao, Z., Patras, I.: Prompting visual-language models for dynamic facial expression recognition. In: *BMVC* (2023) [2](#), [4](#)
54. Zhu, X., Wang, S., Zhu, B., Li, M., Li, Y., Fang, J., Wang, Z., Wang, D., Zhang, H.: Dynamic multimodal prototype learning in vision-language models. In: *Proceedings of the IEEE/CVF international conference on computer vision*. pp. 2501–2511 (2025) [2](#), [4](#)

# Test-Time Adaptation via Cache Personalization for Facial Expression Recognition in Videos Supplementary Materials

Masoumeh Sharafi<sup>1</sup>, Muhammad Osama Zeeshan<sup>1</sup>, Soufiane Belharbi<sup>1</sup>,  
Alessandro Lameiras Koerich<sup>2</sup>, Marco Pedersoli<sup>1</sup>, and Eric Granger<sup>1</sup>

<sup>1</sup> LIVIA, Dept. of Systems Engineering, ETS Montreal, Canada

<sup>2</sup> LIVIA, Dept. of Software and IT Engineering, ETS Montreal, Canada

{masoumeh.sharafi.1,muhammad-osama.zeeshan.1}@ens.etsmtl.ca

{soufiane.belharbi, marco.pedersoli, alessandro.koerich,

eric.granger}@etsmtl.ca

1	Supplementary Algorithms .....	1
2	Experimental Results .....	2
2.1	TTA Baseline Methods .....	2
2.2	Subject-Wise Results .....	3
2.3	Ablation Studies .....	4

## 1 Supplementary Algorithms

This section provides additional algorithmic details for the personalized source-prototype construction and the online test-time adaptation pipeline introduced in the main paper. In particular, we clarify how personalized source prototypes are built from the source subjects and subsequently matched to target subjects, as well as how the proposed online adaptation mechanism operates at inference time on target videos.

Algorithm 1 describes the full procedure used to construct personalized source prototypes. Starting from source-domain embeddings, the method identifies representative subject-specific prototypes for each expression class and transfers them to a target subject through the anchor-class matching strategy described in the main paper. This procedure enables the source cache to better preserve subject-dependent structure while remaining transferable to unseen target subjects. Algorithm 2 summarizes the complete online test-time adaptation pipeline applied to the target video stream. It details the extraction of frame and temporal embeddings, the retrieval of evidence from the personalized source cache and target caches, the embedding-level fusion process, and the cache update mechanism based on the tri-gate rule. Together, these steps illustrate how the proposed method performs efficient and fully online personalization without updating the backbone encoders.

---

**Algorithm 1:** Personalized source-prototype construction

---

**Input:** Source set  $\mathcal{D}^{\text{src}}$ , target set  $\mathcal{D}^{\text{tgt}}$ , frozen image encoder  $E_I$ , classes  $\mathcal{C}$ , anchor class  $c_a$ , top- $m$ , cap  $K$

**Output:** Personalized prototypes  $\mathcal{P}_{t,c}^{\text{pers}}$

**foreach** source subject  $s$  and class  $c \in \mathcal{C}$  **do**

- Extract normalized embeddings  $\mathbf{F}_{s,c}$ ;
- Select DBSCAN parameters;
- if** clustering is invalid or too few samples **then**
- Set  $\mathcal{M}_{s,c}$  to the sample nearest to the class mean;
- else**
- Run DBSCAN on  $\mathbf{F}_{s,c}$ ;
- Set  $\mathcal{M}_{s,c}$  to the medoid of each non-noise cluster;

**foreach** source subject  $s$  **do**

- Compute anchor statistics  $(\mu_s^a, \tilde{\sigma}_s^{2,a})$  from  $\mathcal{M}_{s,c_a}$ ;

**foreach** target subject  $t$  **do**

- Compute anchor statistics  $(\mu_t^a, \tilde{\sigma}_t^{2,a})$  from  $\mathcal{X}_{t,c_a}$ ;
- foreach** source subject  $s$  **do**
- Compute anchor distance  $d(s,t)$ ;
- Select the top- $m$  closest sources  $\mathcal{S}_t$ ;
- foreach** class  $c \in \mathcal{C}$  **do**
- $\mathcal{P}_{t,c}^{\text{pers}} \leftarrow \bigcup_{s \in \mathcal{S}_t} \mathcal{M}_{s,c}$ ;
- if**  $K > 0$  and  $|\mathcal{P}_{t,c}^{\text{pers}}| > K$  **then**
- Keep the  $K$  most relevant prototypes;

**return**  $\{\mathcal{P}_{t,c}^{\text{pers}}\}_{t,c}$ ;

---

## 2 Experimental Results

### 2.1 TTA Baseline Methods

We compare against several CLIP-based test-time adaptation baselines. *TPT* [11] updates only the textual prompt tokens during inference by minimizing prediction entropy over strongly augmented views, while keeping both the image and text encoders frozen. *TDA* [5] is a training-free dynamic adapter that builds a feature-label cache online, progressively refines pseudo-labels, including negative pseudo-labels, and combines cache-based predictions with CLIP zero-shot logits. *DPE* [12] updates visual and textual class prototypes jointly at test time, introduces lightweight sample-specific residuals, and encourages cross-modal consistency between the two prototype spaces under distribution shift. *PromptAlign* [1] adapts prompts by aligning test-time feature statistics with source-domain statistics, thereby reducing distribution mismatch beyond standard entropy-minimization objectives. *ReTA* [6] emphasizes reliable cache-based VLM adaptation through CER (consistency-aware entropy reweighting) for selective cache updates and DDC (diversity-driven distribution calibration), which models each class as a Gaussian family over evolving text embeddings to

**Algorithm 2:** TTA-CaP: online TTA

---

**Input** : Target video  $\mathcal{V}_t^{\text{tgt}} = \{x_t^{\text{tgt}}\}_{t=1}^T$ ; frozen image encoder  $E_I$ ; frozen temporal encoder  $E_t$ ; frozen text encoder  $E_T$ ; class prompts  $\{\tau_c\}_{c \in \mathcal{C}}$ ; personalized source cache  $\mathcal{P}^{\text{src,tgt}}$ ; target caches  $C^{\text{tgt+}}, C^{\text{tgt-}}$ .

**Output:** Video prediction  $\hat{y}$ ; updated target caches  $C^{\text{tgt+}}, C^{\text{tgt-}}$ .

**foreach**  $c \in \mathcal{C}$  **do**

- └ Compute normalized text embedding  $e_c \leftarrow E_T(\tau_c)$

**for**  $t = 1$  **to**  $T$  **do**

- └ Extract frame embedding  $h_t \leftarrow E_I(x_t)$
- └ Compute temporal target embedding  $z_t^{\text{tgt}} \leftarrow \text{POOL}(E_t(h_{t-W+1:t}))$
- └ Normalize  $z_t^{\text{tgt}}$
- └ **foreach**  $c \in \mathcal{C}$  **do**
  - └  $\ell_t^{\text{base}}(c) \leftarrow \eta \cdot \cos(z_t^{\text{tgt}}, e_c)$
- └  $\tilde{y}_t \leftarrow \arg \max_{c \in \mathcal{C}} \ell_t^{\text{base}}(c)$
- └ Compute current-frame entropy  $h_k^{\text{tgt}}$
- └  $(C^{\text{tgt+}}, C^{\text{tgt-}}) \leftarrow \text{TRIGATEUPDATE}(z_k^{\text{tgt}}, \tilde{y}_k^{\text{tgt}}, h_k^{\text{tgt}}, \mathcal{P}^{\text{src,tgt}}, C^{\text{tgt+}}, C^{\text{tgt-}})$
- └ Retrieve source and target cache evidence:
  - └  $z_t^{\text{src,tgt}} \leftarrow \text{RETRIEVESRC}(\mathcal{P}^{\text{src,tgt}}, z_t^{\text{tgt}})$ ,
  - └  $z_t^{\text{tgt+}} \leftarrow \text{RETRIEVEPOS}(C^{\text{tgt+}}, z_t^{\text{tgt}})$ ,  $z_t^{\text{tgt-}} \leftarrow \text{RETRIEVENEG}(C^{\text{tgt-}}, z_t^{\text{tgt}})$
  - └  $z_t^{\text{fuse}} \leftarrow z_t^{\text{tgt}} + z_t^{\text{src,tgt}} + z_t^{\text{tgt+}} - z_t^{\text{tgt-}}$
  - └ Normalize  $z_t^{\text{fuse}}$
  - └ **foreach**  $c \in \mathcal{C}$  **do**
    - └  $\ell_t(c) \leftarrow \eta \cdot \cos(z_t^{\text{fuse}}, e_c)$

$\hat{y} \leftarrow \arg \max_{c \in \mathcal{C}} \frac{1}{T} \sum_{t=1}^T \ell_t(c)$

**return**  $\hat{y}, C^{\text{tgt+}}, C^{\text{tgt-}}$

---

improve calibration. Finally, *T3AL* [7], originally proposed for zero-shot temporal action localization, is adapted here for classification by using video-level pseudo-labels from aggregated frame features, self-supervised refinement of frame-level predictions, and text-guided suppression of irrelevant regions, while keeping the encoders frozen and resetting updates for each sample.

## 2.2 Subject-Wise Results

Tables 1, 2, and 3 report the subject-wise performance across the ten target subjects for each dataset. Each experiment was repeated three times to assess reliability, and the tables report the mean performance with standard deviation over these three trials. These results provide a detailed view of the robustness of each method under subject-level distribution shifts.

On BioVid, most baseline methods show strong performance on certain subjects but suffer noticeable degradation on others, reflecting the difficulty of adapting to individual expression patterns. In contrast, TTA-CaP consistently improves performance for most subjects and achieves the highest overall average

**Table 1:** Subject-wise performance (WAR, UAR) on the BioVid dataset for TTA-CaP and other TTA methods.

Method	Sub-1	Sub-2	Sub-3	Sub-4	Sub-5	Sub-6	Sub-7	Sub-8	Sub-9	Sub-10	Avg.
<b>WAR (%)</b>											
TPT	91.9 ± 0.12	53.0 ± 0.31	50.0 ± 0.00	61.5 ± 0.36	79.0 ± 0.19	88.9 ± 0.14	76.0 ± 0.12	50.0 ± 0.00	98.9 ± 0.05	62.0 ± 0.28	71.1
TDA	93.0 ± 0.10	52.6 ± 0.29	50.0 ± 0.00	63.9 ± 0.32	79.5 ± 0.17	87.5 ± 0.16	76.3 ± 0.18	50.0 ± 0.00	100.0 ± 0.00	61.6 ± 0.26	71.4
DPE	91.7 ± 0.13	55.0 ± 0.27	50.0 ± 0.00	85.0 ± 0.18	73.0 ± 0.24	84.7 ± 0.20	80.0 ± 0.16	50.0 ± 0.00	100.0 ± 0.00	61.8 ± 0.20	73.1
PromptAlign	93.8 ± 0.09	65.2 ± 0.21	50.0 ± 0.00	70.0 ± 0.24	85.0 ± 0.14	92.0 ± 0.10	80.0 ± 0.15	50.0 ± 0.00	100.0 ± 0.00	67.6 ± 0.20	75.3
ReTA	93.8 ± 0.08	65.2 ± 0.19	50.0 ± 0.00	69.5 ± 0.22	85.0 ± 0.13	90.2 ± 0.12	80.0 ± 0.14	50.0 ± 0.00	100.0 ± 0.00	67.6 ± 0.18	75.1
T3AL	94.0 ± 0.07	66.5 ± 0.18	50.0 ± 0.00	70.0 ± 0.21	85.2 ± 0.12	94.2 ± 0.08	83.9 ± 0.13	50.0 ± 0.00	100.0 ± 0.00	67.6 ± 0.17	76.1
<b>TTA-CaP</b>	<b>95.0 ± 0.09</b>	<b>75.0 ± 0.16</b>	<b>50.0 ± 0.00</b>	<b>100.0 ± 0.00</b>	<b>92.5 ± 0.10</b>	<b>97.5 ± 0.06</b>	<b>92.5 ± 0.09</b>	<b>50.0 ± 0.00</b>	<b>100.0 ± 0.00</b>	<b>62.5 ± 0.19</b>	<b>81.5</b>
<b>UAR (%)</b>											
TPT	91.9 ± 0.12	53.0 ± 0.31	50.0 ± 0.00	61.5 ± 0.36	79.0 ± 0.19	88.9 ± 0.14	76.0 ± 0.12	50.0 ± 0.00	98.9 ± 0.05	62.0 ± 0.28	71.1
TDA	93.0 ± 0.10	52.6 ± 0.29	50.0 ± 0.00	63.9 ± 0.32	79.5 ± 0.17	87.5 ± 0.16	76.3 ± 0.18	50.0 ± 0.00	100.0 ± 0.00	61.6 ± 0.26	71.4
DPE	91.7 ± 0.13	55.0 ± 0.27	50.0 ± 0.00	85.0 ± 0.18	73.0 ± 0.24	84.7 ± 0.20	80.0 ± 0.16	50.0 ± 0.00	100.0 ± 0.00	61.8 ± 0.20	73.1
PromptAlign	93.8 ± 0.09	65.2 ± 0.21	50.0 ± 0.00	70.0 ± 0.24	85.0 ± 0.14	92.0 ± 0.10	80.0 ± 0.15	50.0 ± 0.00	100.0 ± 0.00	67.6 ± 0.20	75.3
ReTA	93.8 ± 0.08	65.2 ± 0.19	50.0 ± 0.00	69.5 ± 0.22	85.0 ± 0.13	90.2 ± 0.12	80.0 ± 0.14	50.0 ± 0.00	100.0 ± 0.00	67.6 ± 0.18	75.1
T3AL	94.0 ± 0.07	66.5 ± 0.18	50.0 ± 0.00	70.0 ± 0.21	85.2 ± 0.12	94.2 ± 0.08	83.9 ± 0.13	50.0 ± 0.00	100.0 ± 0.00	67.6 ± 0.17	76.1
<b>TTA-CaP</b>	<b>95.0 ± 0.09</b>	<b>75.0 ± 0.16</b>	<b>50.0 ± 0.00</b>	<b>100.0 ± 0.00</b>	<b>92.5 ± 0.10</b>	<b>97.5 ± 0.06</b>	<b>92.5 ± 0.09</b>	<b>50.0 ± 0.00</b>	<b>100.0 ± 0.00</b>	<b>62.5 ± 0.19</b>	<b>81.5</b>

score. The gains are particularly visible for subjects where baseline methods exhibit larger performance gaps. A similar trend is observed on **StressID**, where subject-specific variability is more pronounced. While baseline methods often fluctuate substantially across subjects, **TTA-CaP** maintains more stable performance and obtains the best average WAR and UAR scores. For **BAH**, the improvements are more moderate due to the dataset’s higher difficulty and the limited discriminative signal reflected in the UAR scores. Nevertheless, **TTA-CaP** still achieves the best average WAR among all methods while maintaining competitive UAR results. Overall, these subject-wise analyses highlight the benefits of the proposed personalized cache construction and tri-gate update strategy, which enables **TTA-CaP** to better adapt to subject-specific characteristics at test time.

### 2.3 Ablation Studies

**Embedding vs. logit fusion.** Fig. 1 reports video-level calibration using reliability diagrams for logit-space and embedding-space fusion. Both curves deviate from the diagonal reference, indicating residual miscalibration, while the curve closer to the diagonal corresponds to better alignment between confidence and empirical accuracy, i.e., lower expected calibration error (ECE) [4]. This comparison highlights how the choice of fusion space affects not only recognition performance but also the reliability of confidence estimates used for downstream decision-making.

**Class prompt selection.** An ablation study was conducted on a diverse set of class-prompt templates commonly used in CLIP-based FER and prompt-based recognition settings [3, 10, 13]. The goal is to assess how the wording of emotion-class prompts affects the quality of text representations and, in turn, downstream recognition performance. These results are obtained using CLIP ViT-B/32, trained on the BioVid source subjects and evaluated on the target subjects. As shown in Table 4, prompt design has a noticeable impact on both WAR and F1 score. Among the evaluated templates, “*a person with an expression*

**Table 2:** Subject-wise performance (WAR, UAR) on the StressID dataset for TTA-CaP and other TTA methods.

Method	Sub-1	Sub-2	Sub-3	Sub-4	Sub-5	Sub-6	Sub-7	Sub-8	Sub-9	Sub-10	Avg.
<b>WAR (%)</b>											
TPT	74.7 $\pm$ 0.18	51.6 $\pm$ 0.21	90.0 $\pm$ 0.09	88.0 $\pm$ 0.12	52.2 $\pm$ 0.24	77.5 $\pm$ 0.11	66.6 $\pm$ 0.22	63.4 $\pm$ 0.19	54.0 $\pm$ 0.23	91.9 $\pm$ 0.08	70.9
TDA	66.9 $\pm$ 0.22	45.2 $\pm$ 0.28	75.6 $\pm$ 0.17	90.1 $\pm$ 0.10	49.6 $\pm$ 0.24	80.0 $\pm$ 0.05	41.2 $\pm$ 0.31	75.3 $\pm$ 0.18	81.8 $\pm$ 0.02	91.9 $\pm$ 0.07	69.7
DPE	64.0 $\pm$ 0.23	55.0 $\pm$ 0.20	73.9 $\pm$ 0.18	90.0 $\pm$ 0.09	52.6 $\pm$ 0.22	80.0 $\pm$ 0.05	50.9 $\pm$ 0.27	73.0 $\pm$ 0.19	81.8 $\pm$ 0.07	92.0 $\pm$ 0.07	71.3
PromptAlign	69.9 $\pm$ 0.20	61.6 $\pm$ 0.17	78.6 $\pm$ 0.14	90.9 $\pm$ 0.08	51.2 $\pm$ 0.21	80.0 $\pm$ 0.15	60.4 $\pm$ 0.19	81.3 $\pm$ 0.13	81.8 $\pm$ 0.06	90.9 $\pm$ 0.09	74.6
ReTA	64.5 $\pm$ 0.21	50.5 $\pm$ 0.23	82.0 $\pm$ 0.12	90.0 $\pm$ 0.09	46.8 $\pm$ 0.25	80.0 $\pm$ 0.12	49.3 $\pm$ 0.29	80.0 $\pm$ 0.04	81.8 $\pm$ 0.10	93.7 $\pm$ 0.06	71.8
T3AL	71.3 $\pm$ 0.18	62.7 $\pm$ 0.16	80.3 $\pm$ 0.13	90.2 $\pm$ 0.08	54.0 $\pm$ 0.20	80.0 $\pm$ 0.07	68.0 $\pm$ 0.17	77.0 $\pm$ 0.14	82.0 $\pm$ 0.05	93.9 $\pm$ 0.06	75.9
TTA-CaP	83.3 $\pm$ 0.14	66.6 $\pm$ 0.15	90.0 $\pm$ 0.08	88.8 $\pm$ 0.10	75.0 $\pm$ 0.16	82.2 $\pm$ 0.09	69.9 $\pm$ 0.18	82.0 $\pm$ 0.07	83.4 $\pm$ 0.06	94.0 $\pm$ 0.05	<b>81.5</b>
<b>UAR (%)</b>											
TPT	70.0 $\pm$ 0.22	55.0 $\pm$ 0.20	90.1 $\pm$ 0.08	79.6 $\pm$ 0.16	59.0 $\pm$ 0.19	77.5 $\pm$ 0.11	50.0 $\pm$ 0.00	54.0 $\pm$ 0.21	52.6 $\pm$ 0.23	56.0 $\pm$ 0.18	64.4
TDA	53.0 $\pm$ 0.24	52.0 $\pm$ 0.22	55.9 $\pm$ 0.19	76.8 $\pm$ 0.17	58.4 $\pm$ 0.20	80.0 $\pm$ 0.07	54.5 $\pm$ 0.26	50.0 $\pm$ 0.00	51.0 $\pm$ 0.24	56.0 $\pm$ 0.17	58.8
DPE	55.4 $\pm$ 0.22	54.8 $\pm$ 0.21	54.9 $\pm$ 0.20	76.9 $\pm$ 0.16	57.0 $\pm$ 0.18	80.0 $\pm$ 0.13	51.0 $\pm$ 0.25	51.0 $\pm$ 0.23	50.0 $\pm$ 0.10	67.0 $\pm$ 0.20	59.8
PromptAlign	55.0 $\pm$ 0.21	54.0 $\pm$ 0.20	61.0 $\pm$ 0.17	81.0 $\pm$ 0.14	53.0 $\pm$ 0.19	80.0 $\pm$ 0.05	60.2 $\pm$ 0.18	65.7 $\pm$ 0.16	50.0 $\pm$ 0.06	50.0 $\pm$ 0.10	61.0
ReTA	54.3 $\pm$ 0.22	51.4 $\pm$ 0.21	61.2 $\pm$ 0.18	75.0 $\pm$ 0.17	51.0 $\pm$ 0.20	80.0 $\pm$ 0.06	55.0 $\pm$ 0.24	61.9 $\pm$ 0.18	50.0 $\pm$ 0.08	61.0 $\pm$ 0.19	60.1
T3AL	56.7 $\pm$ 0.20	60.0 $\pm$ 0.17	62.8 $\pm$ 0.16	82.9 $\pm$ 0.12	54.4 $\pm$ 0.19	80.0 $\pm$ 0.06	62.0 $\pm$ 0.17	77.6 $\pm$ 0.12	54.9 $\pm$ 0.18	65.0 $\pm$ 0.16	65.6
TTA-CaP	85.0 $\pm$ 0.12	62.5 $\pm$ 0.16	70.0 $\pm$ 0.15	87.5 $\pm$ 0.10	62.5 $\pm$ 0.17	87.0 $\pm$ 0.09	75.9 $\pm$ 0.14	90.0 $\pm$ 0.08	65.6 $\pm$ 0.13	97.5 $\pm$ 0.04	<b>78.3</b>

**Table 3:** Subject-wise performance (WAR, UAR) on the BAH dataset for TTA-CaP and other TTA methods.

Method	Sub-1	Sub-2	Sub-3	Sub-4	Sub-5	Sub-6	Sub-7	Sub-8	Sub-9	Sub-10	Avg.
<b>WAR (%)</b>											
TPT	62.0 $\pm$ 0.18	53.7 $\pm$ 0.19	73.9 $\pm$ 0.14	80.0 $\pm$ 0.11	81.2 $\pm$ 0.10	71.0 $\pm$ 0.16	58.0 $\pm$ 0.17	55.0 $\pm$ 0.18	69.0 $\pm$ 0.15	53.0 $\pm$ 0.20	65.6
TDA	58.0 $\pm$ 0.20	53.7 $\pm$ 0.18	75.0 $\pm$ 0.13	80.3 $\pm$ 0.10	79.0 $\pm$ 0.12	71.6 $\pm$ 0.15	58.0 $\pm$ 0.16	55.9 $\pm$ 0.17	69.0 $\pm$ 0.14	51.7 $\pm$ 0.22	65.2
DPE	58.6 $\pm$ 0.19	59.6 $\pm$ 0.16	79.6 $\pm$ 0.10	80.5 $\pm$ 0.10	83.4 $\pm$ 0.09	67.0 $\pm$ 0.18	59.0 $\pm$ 0.15	54.0 $\pm$ 0.19	71.9 $\pm$ 0.12	54.0 $\pm$ 0.18	66.7
PromptAlign	59.1 $\pm$ 0.18	59.1 $\pm$ 0.16	72.0 $\pm$ 0.15	84.5 $\pm$ 0.09	84.1 $\pm$ 0.08	72.4 $\pm$ 0.14	58.5 $\pm$ 0.16	55.9 $\pm$ 0.17	71.5 $\pm$ 0.12	54.9 $\pm$ 0.17	67.1
ReTA	61.4 $\pm$ 0.17	60.0 $\pm$ 0.15	72.0 $\pm$ 0.14	84.0 $\pm$ 0.09	84.1 $\pm$ 0.08	72.4 $\pm$ 0.13	58.5 $\pm$ 0.15	55.9 $\pm$ 0.16	72.0 $\pm$ 0.11	56.0 $\pm$ 0.16	67.6
T3AL	61.0 $\pm$ 0.17	58.9 $\pm$ 0.16	75.0 $\pm$ 0.13	85.6 $\pm$ 0.08	83.6 $\pm$ 0.09	74.7 $\pm$ 0.12	60.0 $\pm$ 0.14	56.0 $\pm$ 0.15	71.0 $\pm$ 0.12	53.6 $\pm$ 0.18	67.9
TTA-CaP	62.5 $\pm$ 0.16	62.1 $\pm$ 0.14	79.6 $\pm$ 0.09	85.8 $\pm$ 0.07	84.4 $\pm$ 0.08	75.2 $\pm$ 0.11	60.1 $\pm$ 0.13	56.6 $\pm$ 0.14	70.0 $\pm$ 0.13	56.6 $\pm$ 0.15	<b>69.2</b>
<b>UAR (%)</b>											
TPT	51.0 $\pm$ 0.08	50.0 $\pm$ 0.00	50.0 $\pm$ 0.04	50.0 $\pm$ 0.05	51.0 $\pm$ 0.08	53.1 $\pm$ 0.12	50.0 $\pm$ 0.05	49.0 $\pm$ 0.10	50.0 $\pm$ 0.00	50.0 $\pm$ 0.00	50.4
TDA	50.0 $\pm$ 0.05	50.0 $\pm$ 0.00	50.0 $\pm$ 0.04	51.0 $\pm$ 0.08	50.0 $\pm$ 0.05	50.0 $\pm$ 0.04	50.0 $\pm$ 0.05	50.0 $\pm$ 0.04	50.0 $\pm$ 0.00	50.0 $\pm$ 0.00	50.1
DPE	50.0 $\pm$ 0.04	50.0 $\pm$ 0.00	50.0 $\pm$ 0.04	50.0 $\pm$ 0.05	50.0 $\pm$ 0.04	50.0 $\pm$ 0.04	50.0 $\pm$ 0.05	50.0 $\pm$ 0.04	50.0 $\pm$ 0.00	50.0 $\pm$ 0.00	50.0
PromptAlign	50.0 $\pm$ 0.04	50.0 $\pm$ 0.00	50.2 $\pm$ 0.05	51.8 $\pm$ 0.09	50.0 $\pm$ 0.04	50.0 $\pm$ 0.04	50.0 $\pm$ 0.05	50.0 $\pm$ 0.04	50.0 $\pm$ 0.00	50.0 $\pm$ 0.00	50.2
ReTA	50.0 $\pm$ 0.04	50.0 $\pm$ 0.00	50.2 $\pm$ 0.05	51.8 $\pm$ 0.09	50.0 $\pm$ 0.04	50.0 $\pm$ 0.04	50.0 $\pm$ 0.05	50.0 $\pm$ 0.04	50.0 $\pm$ 0.00	50.0 $\pm$ 0.00	50.2
T3AL	51.4 $\pm$ 0.08	50.0 $\pm$ 0.00	50.0 $\pm$ 0.04	50.0 $\pm$ 0.05	51.4 $\pm$ 0.08	54.0 $\pm$ 0.11	54.3 $\pm$ 0.10	50.0 $\pm$ 0.04	50.0 $\pm$ 0.00	50.0 $\pm$ 0.00	<b>51.1</b>
TTA-CaP	51.5 $\pm$ 0.07	50.0 $\pm$ 0.00	50.0 $\pm$ 0.04	50.0 $\pm$ 0.05	51.0 $\pm$ 0.08	53.0 $\pm$ 0.10	50.0 $\pm$ 0.05	50.0 $\pm$ 0.04	50.0 $\pm$ 0.00	50.0 $\pm$ 0.00	50.5

of  $[CLS]$ ” yields the best overall performance and is therefore adopted in all methods that rely on class prompts.

**Ablation on source cache construction** Alternative strategies for constructing the static personalized source cache are compared while keeping the online TTA pipeline and cache budget fixed. As a simple baseline, a single prototype is selected per (subject, class) by applying k-means clustering [8, 9] with  $k=1$  (i.e., the closest sample to the class centroid). Next, a two-stage clustering strategy is evaluated, where prototypes are first selected per (subject, class) and then re-clustered after pooling across subjects to produce a compact class-level cache; both k-means and DBSCAN [2] are considered in this second clustering step. Finally, fully personalized prototype selection is considered by retaining subject-specific clusters (k-means/DBSCAN) instead of pooling across subjects. Table 5 shows that increasing prototype diversity and personalization consistently improves WAR: the  $k=1$  baseline achieves 78.8 WAR, two-stage clustering provides modest gains (79.3–79.5), and personalized clustering yields further improve-

**Table 4:** Ablation of class-prompt templates for the CLIP text encoder on BioVid using CLIP ViT-B/32. Performance varies noticeably across prompt formulations, and the template “a person with an expression of [CLS]” achieves the best WAR and F1 score.

Prompt Template	WAR	F1 score
a photo of a [CLS]	68.7	63.3
a_photo_of_the_[CLS]_face	66.5	59.3
a_photo_of_one_[CLS]_face	64.2	55.8
a_close-up_photo_of_the_[CLS]_face	68.2	62.6
a_low_resolution_photo_of_a_[CLS]_face	68.7	64.2
a_good_photo_of_a_[CLS]_face	69.2	65.4
a_photo_of_my_[CLS]_face	66.2	60.3
a_cropped_photo_of_the_[CLS]_face	64.5	57.5
a_photo_of_a_person_with_[CLS]_face	67.2	61.4
<b>a person with an expression of [CLS]</b>	<b>69.7</b>	<b>66.6</b>
a_portrait_of_a_person_in_[CLS]	58.2	46.7
a_face_showing_signs_of_[CLS]	68.7	64.1
a close up portrait of a [CLS] expression	69.2	63.0
a realistic photo of a person experiencing [CLS]	53.5	40.0
a cropped image of a person in [CLS]	69.0	64.5
a photo of a [CLS] person	69.5	64.3
a person with a facial expression of [CLS]	69.5	64.2
a high quality photo of a [CLS] expression	69.5	64.3
a photo of a face showing [CLS]	69.5	64.3
a photo of a face in [CLS]	69.0	61.8

**Table 5:** Effect of different static source-cache construction strategies. Average WAR (%) over target subjects in BioVid using TTA-CaP.

Cache construction	WAR (%) $\uparrow$
Baseline (k-means, $k=1$ )	78.8
Two-stage (k-means)	79.3
Two-stage (DBSCAN)	79.5
Personalized (k-means)	79.6
Personalized (DBSCAN)	<b>81.0</b>

ments, with personalized DBSCAN achieving the best result of 81.7 WAR. Overall, the results indicate that preserving subject-specific structure in the source cache is beneficial under domain shift.

## References

1. Abdul Samadh, J., Gani, M.H., Hussein, N., Khattak, M.U., Naseer, M.M., Shahbaz Khan, F., Khan, S.H.: Align your prompts: Test-time prompting with dis-

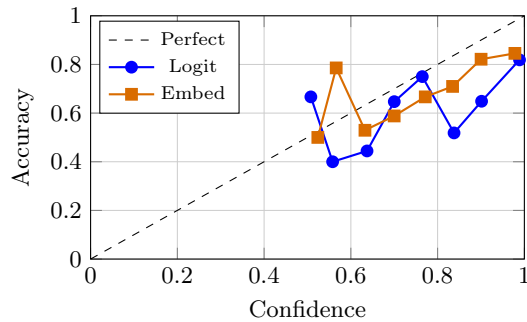


**Fig. 1:** Video-level reliability diagram; lower ECE indicates better alignment between confidence and empirical accuracy (avg distance to the line).

- tribution alignment for zero-shot generalization. *Advances in Neural Information Processing Systems* **36**, 80396–80413 (2023) [2](#)
2. Ester, M., Kriegel, H.P., Sander, J., Xu, X., et al.: A density-based algorithm for discovering clusters in large spatial databases with noise. In: *kdd*. vol. 96, pp. 226–231 (1996) [5](#)
  3. Foteinopoulou, N.M., Patras, I.: Emoclip: A vision-language method for zero-shot video facial expression recognition. In: *2024 IEEE 18th International Conference on Automatic Face and Gesture Recognition (FG)*. pp. 1–10. IEEE (2024) [4](#)
  4. Guo, C., Pleiss, G., Sun, Y., Weinberger, K.Q.: On calibration of modern neural networks. In: *International conference on machine learning*. pp. 1321–1330. PMLR (2017) [4](#)
  5. Karmanov, A., Guan, D., Lu, S., El Saddik, A., Xing, E.: Efficient test-time adaptation of vision-language models. In: *Proceedings of the IEEE/CVF Conference on Computer Vision and Pattern Recognition*. pp. 14162–14171 (2024) [2](#)
  6. Liang, Y., Chen, H., Xiong, Y., Zhou, Z., Lyu, M., Lin, Z., Niu, S., Zhao, S., Han, J., Ding, G.: Advancing reliable test-time adaptation of vision-language models under visual variations. In: *Proceedings of the 33rd ACM International Conference on Multimedia*. pp. 4788–4797 (2025) [2](#)
  7. Liberatori, B., Conti, A., Rota, P., Wang, Y., Ricci, E.: Test-time zero-shot temporal action localization. In: *Proceedings of the IEEE/CVF conference on computer vision and pattern recognition*. pp. 18720–18729 (2024) [3](#)
  8. Lloyd, S.: Least squares quantization in pcm. *IEEE transactions on information theory* **28**(2), 129–137 (1982) [5](#)
  9. McQueen, J.B.: Some methods of classification and analysis of multivariate observations. In: *Proc. of 5th Berkeley Symposium on Math. Stat. and Prob.* pp. 281–297 (1967) [5](#)
  10. Ni, B., Peng, H., Chen, M., Zhang, S., Meng, G., Fu, J., Xiang, S., Ling, H.: Expanding language-image pretrained models for general video recognition. In: *European Conference on Computer Vision*. pp. 1–18 (2022) [4](#)
  11. Shu, M., Nie, W., Huang, D.A., Yu, Z.: Test-time prompt tuning for zero-shot generalization in vision-language models. *Advances in Neural Information Processing Systems* **35**, 14274–14289 (2022) [2](#)

12. Zhang, C., Stepputtis, S., Sycara, K., Xie, Y.: Dual prototype evolving for test-time generalization of vision-language models. *Advances in Neural Information Processing Systems* **37**, 32111–32136 (2024) [2](#)
13. Zhao, Z., Cao, Y., Gong, S., Patras, I.: Enhancing zero-shot facial expression recognition by llm knowledge transfer. in *2025 ieee/cvf winter conference on applications of computer vision (wacv)* (2025) [4](#)